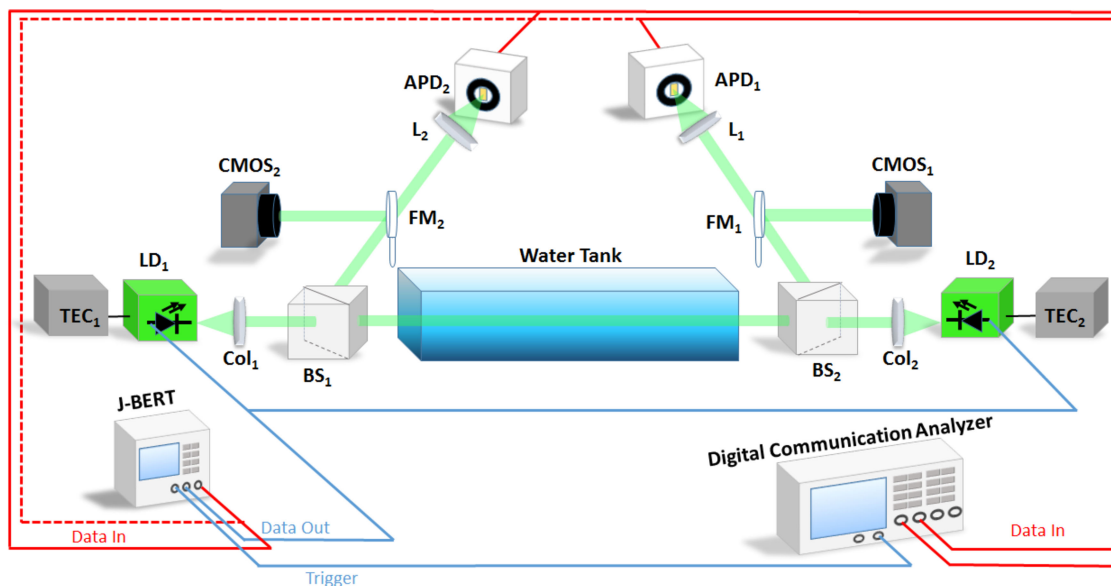


On the Reciprocity of Underwater Turbulent Channels



Volume 11, Number 2, April 2019

Yujian Guo
Abderrahmen Trichili
Omar Alkhazragi
Islam Ashry
Tien Khee Ng
Mohamed-Slim Alouini
Boon S. Ooi



DOI: 10.1109/JPHOT.2019.2898094
1943-0655 © 2019 IEEE

On the Reciprocity of Underwater Turbulent Channels

Yujian Guo , Abderrahmen Trichili , Omar Alkhazragi ,
Islam Ashry , Tien Khee Ng , Mohamed-Slim Alouini ,
and Boon S. Ooi 

Computer, Electrical and Mathematical Sciences and Engineering Division, King Abdullah
University of Science and Technology, Thuwal 23955-6900, Saudi Arabia

DOI:10.1109/JPHOT.2019.2898094

1943-0655 © 2019 IEEE. Translations and content mining are permitted for academic research only.
Personal use is also permitted, but republication/redistribution requires IEEE permission.
See http://www.ieee.org/publications_standards/publications/rights/index.html for more information.

Manuscript received December 25, 2018; revised February 1, 2019; accepted February 1, 2019. Date of publication February 12, 2019; date of current version March 5, 2019. This work was supported by the King Abdullah University of Science and Technology under baseline funding BAS/1/1614-01-01, KAUST finding KCR/1/2081-01-01, and KAUST funding GEN/1/6607-01-01. Corresponding author: Boon S. Ooi (e-mail: boon.ooi@kaust.edu.sa).

Abstract: Through a series of experiments incorporating two counter-propagating communication channels, we investigate the reciprocity nature of underwater turbulence. Bit error rate measurement and statistical data analysis reveal a high reciprocal nature of turbulence induced by the presence of bubbles, temperature, and salinity. We further demonstrate the effect of distortions at the beam level that could potentially be used for underwater communication system design considerations.

Index Terms: Underwater wireless optical communication, underwater propagation, oceanic turbulence, channel reciprocity.

1. Introduction

High-Bit-Rate underwater wireless optical communication (UWOC) has lately received a considerable attention since it offers low latency and good stealth, which can complement acoustic wave communication [1], [2]. Several reports have shown that UWOC can be efficiently adopted to deliver information underwater with high fidelity over short and moderate distances up to several tens of meters [3]–[6]. Scenarios that involve air-water communications were also proposed [7], [8]. Recent studies have further reported the use of multiple spatial modes of light to establish underwater communication links [9]–[11]. The performance of UWOC is strongly correlated to channel conditions in a manner similar to the effect of atmospheric turbulence on free space optical communication (FSO) [12]. Atmospheric turbulence, as a major concern for FSO, has been well studied in the literature [12]. The study of the effects of various underwater conditions, including temperature, salinity and the presence of bubbles, on the performance of optical wireless communication systems have just begun to gain momentum [13]–[17]. Much investigations and explorations are required to further quantify and qualify the impact of underwater turbulence on the performance of UWOC communications to benefit practical deployment of UWOC systems.

Theoretical studies in the '70s revealed that atmospheric turbulence has a reciprocal nature [18], [19], meaning that two laser beams propagating in opposite directions experience the same atmospheric turbulence distortions. Atmospheric turbulence reciprocity has been later confirmed

experimentally [20], [21]. Through reciprocity in FSO, a pilot signal from a receiver can be used at the transmitter end to provide channel state information (CSI), based on which the transmitter end could employ various digital signal processing (DSP) techniques. This includes adaptive modulation and coding, and varying the system bit rate [18]. Reciprocity is also a key characteristic based on which beam-phase and amplitude pre-correction can be performed through adaptive optics (AO). By exploiting the channel reciprocity characteristic, communication systems can be designed to cope with complexity and latency issues and ultimately improve the performance of FSO-based communications [22]. Similarly, investigating the reciprocity nature of an underwater channel in the presence of turbulence is crucial. However, this has yet to receive the well-deserved attention. If underwater channel reciprocity holds, no continuous feedback is needed to bring CSI to the transmitter to adapt the transmission signals to channel conditions and get better received signals at the receiver. In this work, we experimentally emulate and investigate the effect of underwater turbulence due to turbidity, bubbles, temperature inhomogeneity, and salinity on the channel reciprocity. Throughout the paper, we also provide beam profile analysis that could be helpful when designing underwater communication links subject to turbulence.

2. Concept and Experimental Methodology

While propagating in water in the z axis, the intensity of a light signal, I , decays exponentially following Beer's law expressed as follows:

$$I = I_0 \exp(-c(\lambda)z), \quad (1)$$

where I_0 is the light intensity at $z = 0$, $c(\lambda)$ denotes the attenuation coefficient measured in m^{-1} and depends to the wavelength λ . The attenuation coefficient $c(\lambda)$ is obtained by summing two different quantities $\alpha(\lambda)$ and $b(\lambda)$ which represent the absorption and scattering coefficients, respectively. Due to absorption, the intensity of two beams following the same path in opposite directions will decay in an identical manner. Water scattering also fulfill the principle of reciprocity [23]. In addition to the attenuation due to water absorption and scattering, performance of such communication depends on the underwater environment which is still a major concern. Underwater turbulence affects light propagation due to the changes in refractive index associated with fluctuations in temperature and salinity. UWOC can be also subject to air bubbles that could be mainly produced by breaking surface waves and air [25].

As shown in Fig. 1, our experimental investigation involves two beams produced by two identical lasers propagating through a 1.2-m-long tank filled with pure water type I from water deionizer (MilliQ Academic) to establish two overlapped channels in opposite directions. Both beams are horizontally superimposed such that they experience the same underwater conditions at the same water level.

The transmission side of each of the counter-propagating links comprised of a 520-nm green single mode fiber pigtailed laser diode (Thorlabs LP520-SF15) that is current-driven through a temperature controller (Thorlabs ITC 4000 series) and mounted on a LD/TEC mount (Thorlabs LDM9LP). At the reception side, a high-speed Si avalanche photodetector (APD) (Menlo systems APD 210) is used for each light channel. As shown in Fig. 1, we further include two 50:50 non-polarizing beam splitters to ensure the superposition of the two channels. The signal transmitted by LD₁ (LD₂) and detected by APD₁ (APD₂) is denoted by channel 1 (channel 2). Each laser is modulated using 1 Gbps OOK signals generated by a high-performance bit error rate (BER) tester (Agilent Technologies J-BERT N4903B). In the disturbance-free case, the bit error rate of each channel in our system equals to 10^{-10} . Both lasers are set to emit continuous-wave (CW) 6 mW optical power. The APD receives 0.6 mW optical power at each side along channel 1 and channel 2.

3. Results and Discussion

We start with investigating the turbidity reciprocity by installing two tubes at each end of the tank, connected to two pumps to circulate the inside water. When the pumps are on, water flow is

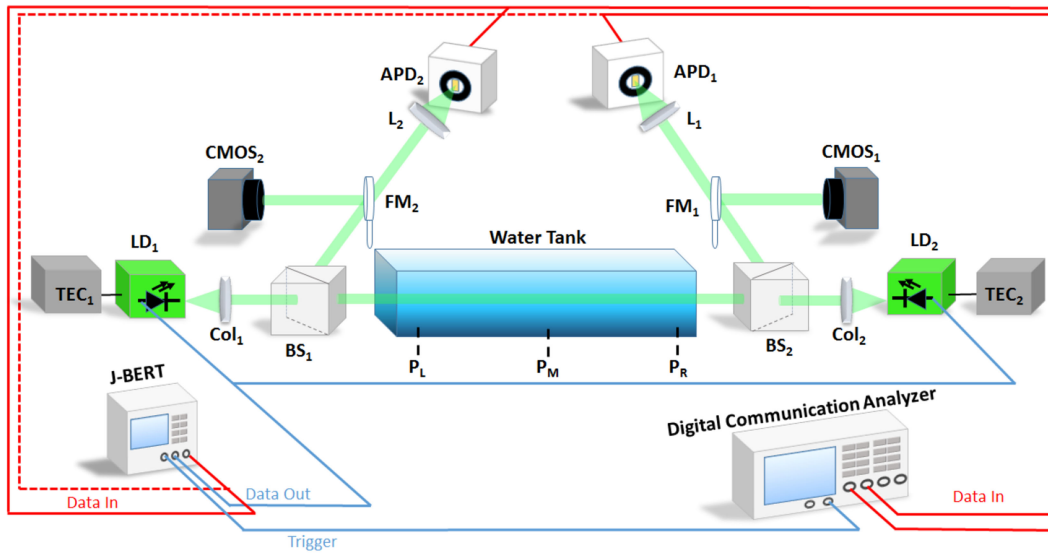


Fig. 1. Experimental setup of underwater turbulence reciprocity investigation. TEC: temperature controller; LD: laser diode; BS: beam splitter; Col: collimator; CMOS: camera; FM: flip mirror; APD: avalanche photodetector; L_1 , L_2 are 35-mm focal length lenses.

generated which is found to have no significant effect on the BER performance for both links and it remains stable at 10^{-10} .

As shown in Figs. 2(a)–2(d), by comparing the histograms of channel 1 and channel 2 at clear water, obtained using 10,000 samples divided to the mean value of the samples, with those calculated under the effect of turbidity, one can conclude that there is no significant effect of the water motion on the performance of both channels due to the homogeneity of the medium. We should stress that the direction of flow in homogeneous and constant index of refraction water has a limited effect on both channels. We also collect the scintillation index (SI), σ_I^2 , defined as the variance of normalized intensity fluctuations at the APD and given as follows:

$$\sigma_I^2 = \frac{E[I^2] - E^2[I]}{E[I]^2}, \quad (2)$$

where I is the collected intensity and $E[I]$ is the expected value of the intensity. σ_I^2 has been widely considered as a key metric for the performance of optical wireless communications [26]. The σ_I^2 collected for channel 1 and channel 2 are, respectively, equal to 0.497 and 0.503. The received optical powers by both APDs remain constant at the level of 0.6 mW. Although it has a very weak effect in homogeneous water, turbidity demonstrates a high reciprocal nature. We also believe that the slight difference between the histograms and the scintillation indices is due to slight misalignment or the slight difference in sensitivity between the APDs used to collect the intensity of the two light signals.

Moving to bubbles effect investigation, we place an N_2 -gas tube in the middle of the tank (position marked as P_M in Fig. 1) to generate bubbles in a uniform manner for the two beams. For a weak bubbles regime corresponding to a gas flow rate of 1 mL/s, we report accumulated BER values, over a 5-minute time window, of 2.741×10^{-7} for channel 1 and of 2.210×10^{-7} for channel 2. The SI values for channel 1 and channel 2 are 0.556 and 0.624, respectively. We note that in general a higher SI value reflects higher scintillation (fluctuation) of the channel caused by underwater turbulence. In our case, the optical scintillation of the channel is represented by the electrical signal intensity converted from the optical signal by the APD and here we simply compare the change of the SI values between different scenarios which can reflect the changes of the channel performance and the effect of turbulence on the communication link. In order to quantitatively

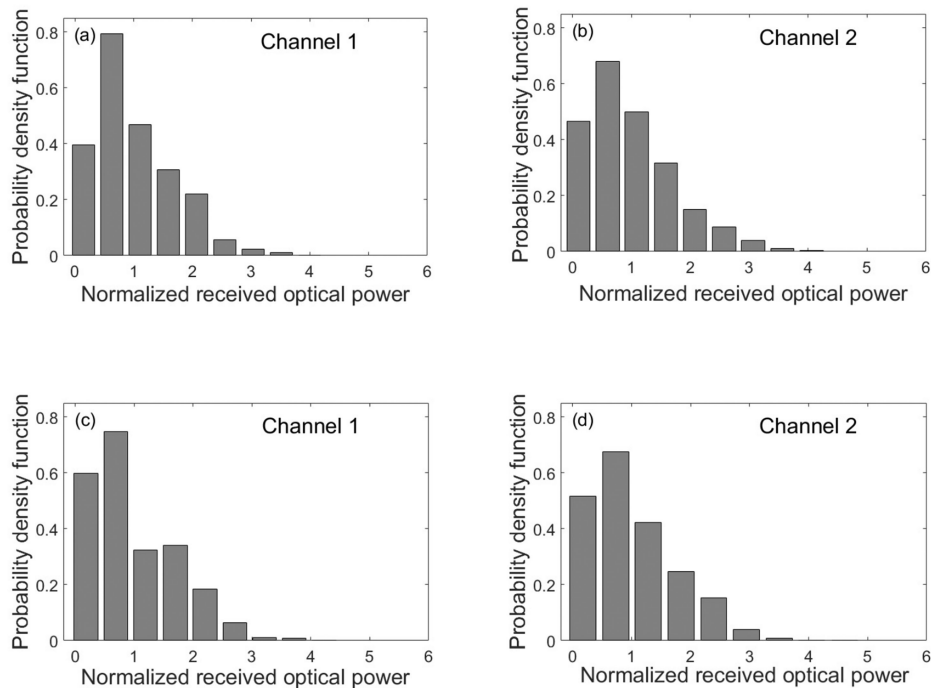


Fig. 2. Histograms of the measured power for channel 1 and channel 2 (a, b) at clear water corresponding to the non-turbulence case and (c, d) at turbid water.

measure the goodness of fit between the intensity fluctuations histograms of the two channels, we use a correlation coefficient denoted as R^2 [27]. R^2 is calculated as follows:

$$R^2 = 1 - \frac{SSE}{SST}, \quad (3)$$

where SSE is the sum of square errors with one of the histograms being the reference set of measurements and SST is the sum total of the squares of difference between the measured points and the mean value. R^2 ranges between 0 and 1 which generally increases with the goodness of fit. R^2 is unity when there is a perfect matching between the two histograms and it equals zero if there is no similarity between them. The relation of the two histograms of channel 1 and channel 2, shown in Figs. 3(a) and 3(b), produces $R^2 = 0.985$. For a strong bubbles regime, that corresponds to 2.84 mL/s, the accumulated BER values for channel 1 and channel 2 are, respectively, 4.250×10^{-6} and 2.230×10^{-6} . σ_I^2 values are equal to 0.613 and 0.633 for channel 1 and channel 2, respectively. We then change the position of the N_2 tube in the tank twice to the left end and the right end, marked, respectively, in Fig. 1 as P_L and P_R . In Figs. 3(a)–3(f), the histograms of channel 1 and channel 2, at different positions of the bubbles tube inside the tank, are presented. Key performances, BER and SI, of the two optical channels, as well as the R^2 coefficients collected at different positions of the bubbles tube are presented in Table 1. The values of the BER and SI in Table 1 show that the position of the bubbles has no considerable effect on the performance of the two channels. Comparing the results of the two channels reveals a high reciprocal nature of bubble-induced turbulence. To visualize the effect of air bubbles at the beam level, we use a Thorlabs CMOS camera (DCC1645C) to capture the beam profiles emitted by LD₁ after propagating through the bubbly water (Fig. 4).

As observed in Figs. 4(b) and 4(c), the beam profiles are shadowed by the air bubbles which partially or almost completely obstruct the beam depending on the flow of the air. The bubbles when projected on the CMOS camera appeared flatter rather than circular which is due to the forces applied by the water molecules on the air bubbles that cannot be perfectly spherical. We

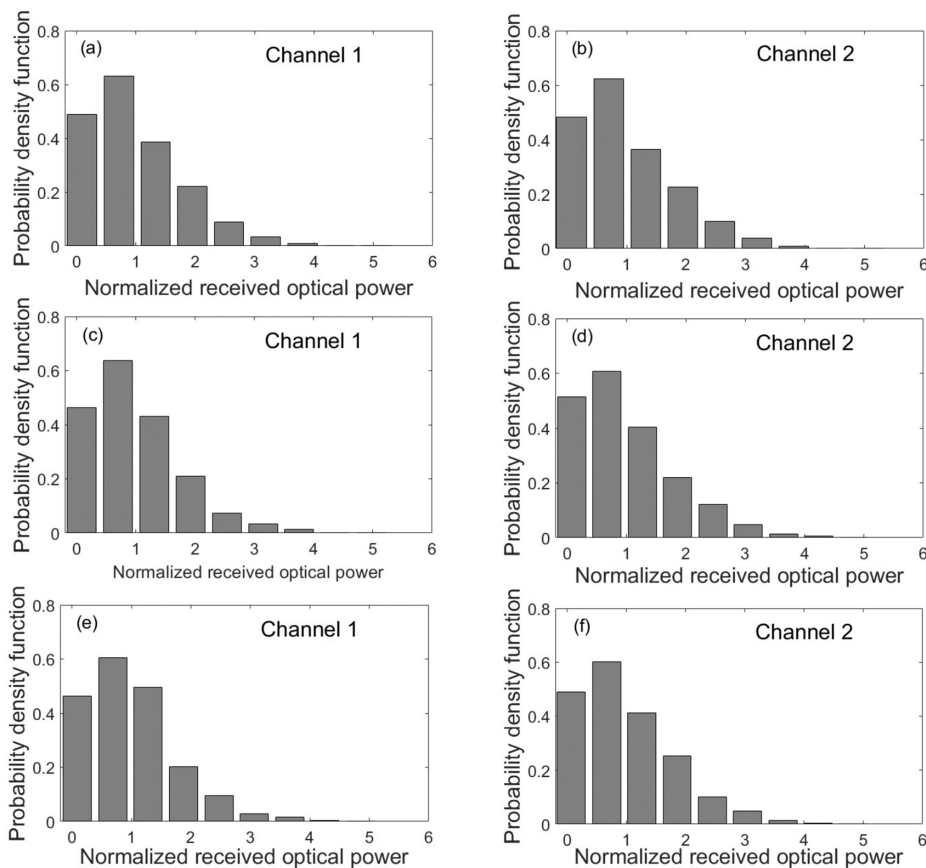


Fig. 3. Histograms of the measured power for channel 1 and channel 2 for a flow rate of 1 mL/s at tank positions (a, b) P_M , (c, d) P_L and (e, f) P_R .

believe that beams with large profiles, that can be possibly formed using a beam expander, may perform better than beams with relatively small profiles as demonstrated by [16].

To study the effect of changing the water temperature on the channel reciprocity, different case scenarios are considered including propagating the beams between two separated regions of water with different temperatures, mixing water with different temperatures, and creating a vertical thermal gradient. As shown in Fig. 5, we start by dividing the water tank into two regions with different temperatures separated by an acrylic board of 4 mm thickness that transmits up to 92% of visible light. The water temperature of the tank left side is set to 20.6 °C, while for the right side is increased by 5, 6, and 7 °C. While propagating a beam emitted by LD₁ through the two water regions, the BER performance remains stable and the accumulated BER over a time window of 5 minutes is, respectively, equal to 0.665×10^{-6} , 0.427×10^{-6} , and 0.319×10^{-6} at 5, 6, and 7 °C temperature difference. Similar results were obtained for LD₂. Histograms that are presented in Figs. 6(a) and 6(b) demonstrate strong similarity between the effect of separating temperature for channel 1 and channel 2. Measured beam profile at a temperature difference of 5 °C is presented in Fig. 7(a).

We then remove the separation board to mix water from both water regions of the tank. Once the water of both regions is mixed, the beam becomes distorted as shown in Fig. 7(b). The BER performance for both channels degrades drastically and the instantaneous values reaches the forward error correction (FEC) limit. The shape of the beam profile is changing according to the water motion and the temperature inhomogeneity. We note that variation of the refractive index of the water is governed by the variation of temperature [28], and therefore temperature inhomogeneity

TABLE 1
BER, SI, and R^2 Calculated for Channels 1 and 2 When Bubbles Are Formed Within the Tank

Method	Location	Laser	BER		SI	R^2
			1 min	5 min		
No Bubbles		LD ₁	1.720×10^{-9}	8.070×10^{-10}	0.497	0.956
		LD ₂	3.810×10^{-10}	7.680×10^{-10}	0.503	
1 mL/s	P _R	LD ₁	2.391×10^{-6}	2.260×10^{-6}	0.533	0.978
		LD ₂	6.760×10^{-7}	6.640×10^{-7}	0.594	
	P _L	LD ₁	2.978×10^{-7}	5.250×10^{-7}	0.560	0.998
		LD 2	1.714×10^{-6}	2.051×10^{-6}	0.609	
	P _M	LD ₁	2.695×10^{-7}	2.741×10^{-6}	0.556	0.985
		LD ₂	1.278×10^{-7}	2.210×10^{-7}	0.624	
2.84 mL/s	P _R	LD ₁	4.900×10^{-6}	5.240×10^{-6}	0.573	0.968
		LD ₂	6.430×10^{-7}	3.016×10^{-7}	0.592	
	P _L	LD ₁	4.640×10^{-6}	4.620×10^{-6}	0.644	0.929
		LD ₂	2.768×10^{-6}	6.900×10^{-7}	0.602	
	P _M	LD ₁	4.340×10^{-6}	4.250×10^{-6}	0.617	0.908
		LD ₂	1.780×10^{-6}	2.230×10^{-6}	0.633	

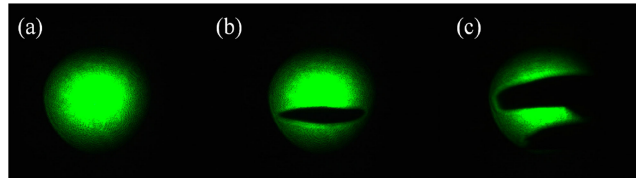


Fig. 4. (a) Measured beam profile at clear water. Beam under (b) low and (c) moderately high-bubbles regimes.

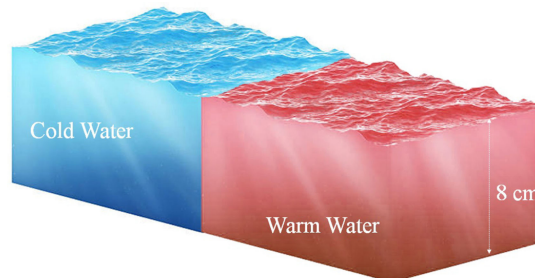


Fig. 5. A schematic illustrating the horizontal thermal separation.

creates a non-uniformity of the water refractive index which leads to beam wandering that degrades the overall performance of the underwater channel [24]. When the water starts to settle down, the lower temperature water descends to the bottom of the tank while the higher temperature water resides at the top which is related to water density that is inversely proportional to the temperature. A middle status of temperature distribution of water that we describe as a vertical

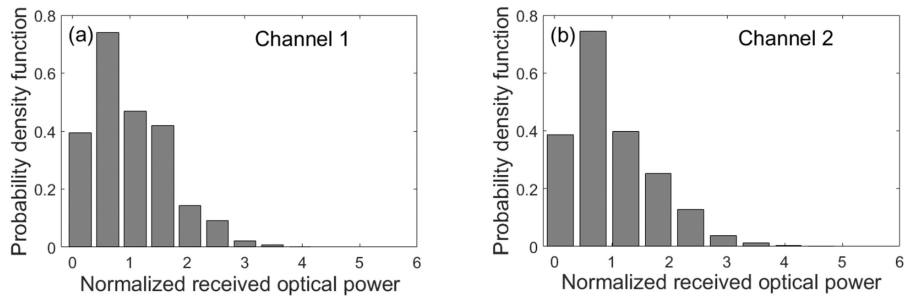


Fig. 6. Histograms of the measured power for (a) channel 1 and (b) channel 2 when passing through a temperature separation region.

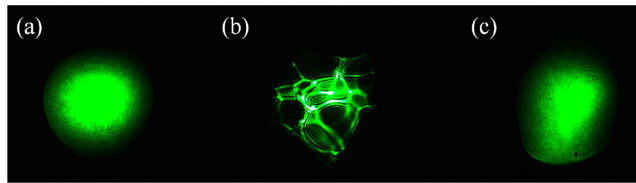


Fig. 7. Measured beam profiles propagating (a) from cold to hot water, (b) at turbid non-homogeneous water. (c) Beam expansion due to a vertical thermal gradient.

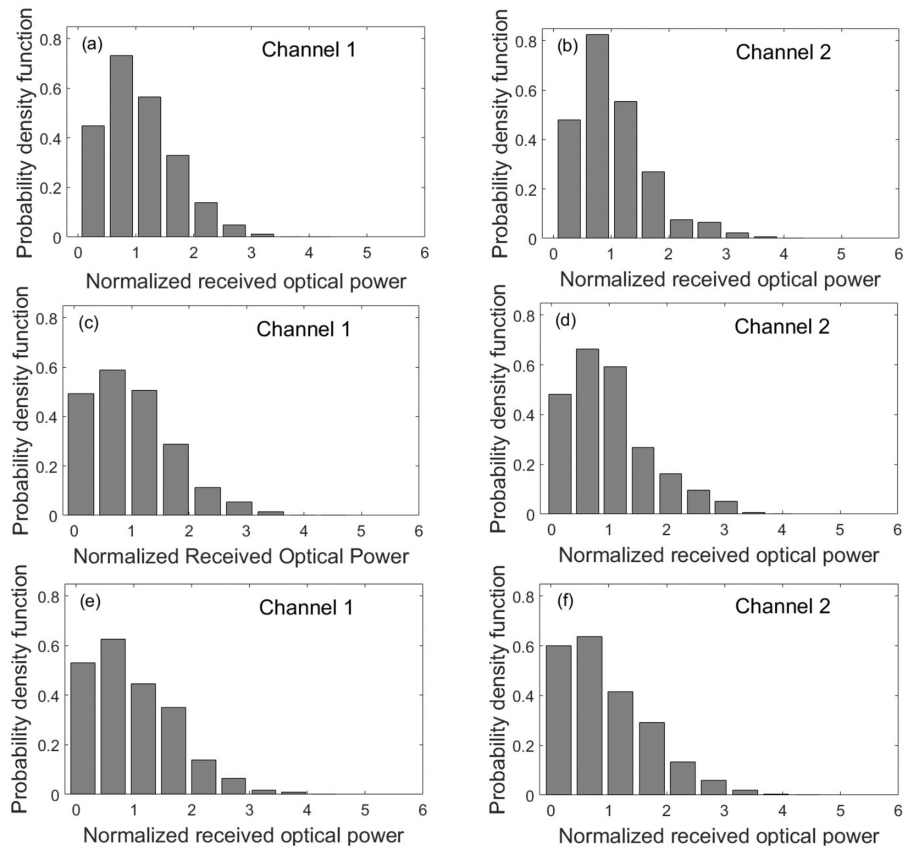


Fig. 8. Histograms of the measured power for channel 1 and channel 2 at salt concentration of (a, b) 8.33 g/L at clear water and (c, d) 16.67 g/L. (e, f) Same salt concentration as (c, d) and taking into account the effect of turbidity.

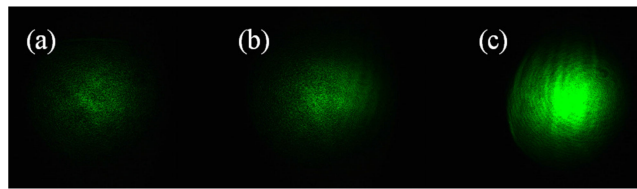


Fig. 9. Effect of salinity on the laser beam at (a) strong water turbidity and (b) moderate water turbidity for a 16.67 g/L salt concentration. (c) Laser beam at 8.33 g/L salt concentration with no turbidity.

temperature gradient is created. As seen in Fig. 7(c), the beam profile expands and is shifted down due to the non-homogeneity of the refractive index of the water along the vertical axis. The vertical thermal gradient strength is measured, when the beam profile is captured, and is found to be equal to 0.1 °C/cm with 21.6 °C on the top of the tank and 20.8 °C at the bottom. After 15 minutes, the water temperature becomes homogeneous and the beam shape recovers to the case of no-turbulence as well as the BER performance for the two superimposed communication channels.

Next, we investigate the effect of salinity. The water inside the tank has now a salt concentration of 8.33 g/L. The received powers for both APD sides are reduced to 0.58 mW. However, the BER performance remains acceptable at a level of 1.00×10^{-6} for channel 1 and 1.01×10^{-6} for channel 2. The SI values for channel 1 and channel 2 are 0.565 and 0.601, respectively. For a higher salt concentration of 16.67 g/L, the received powers for channel 1 and for channel 2 are reduced to 0.36 mW. SI values are increased to reach 0.638 for channel 1 and 0.602 for channel 2. The BER performance for the two channels remains at the level of 10^{-6} . This can be explained by the fact that salinity mainly increases the attenuation and by doubling the salt concentration we have enough power to deliver a similar performance to the 8.33 g/L case. Measured received power histograms for the two salt concentrations are presented in Fig. 8(a)–8(d). In Figs. 8(e) and 8(f), we demonstrate the power histograms for a water salt concentration of 16.67 g/L when the effect of turbidity due to water circulating pumps is considered.

The salinity-induced turbulence seems to have a reciprocal nature with and without water turbidity. By keeping the same salinity concentration and changing the effect of turbidity, the attenuation effect of water increases significantly as can be seen from the beam images at different turbidity conditions presented in Figs. 9(a) and 9(b). In Fig. 9(c), a clear beam profile is obtained at low salt concentration in clear water.

4. Conclusion

In summary, we experimentally describe the study of the reciprocal nature of underwater turbulence effects caused by the turbidity, air bubbles, temperature variations, and salinity. By analyzing the BER performance, SI values, and power histograms, from the similar turbulence effect of two channels, the reciprocal nature of underwater turbulence is proven. It is worth mentioning that small difference in measured statistical parameters and BER could be due to the non-perfect reciprocity of the used devices due to calibration or manufacturing imperfections. To improve the performance of underwater communication system, we note that the effects of turbulence should be taken into account when designing the communication links. Several techniques that have been widely used in free space optics can be used for UWOC. Beam tracking can be used in the case of large vertical thermal gradient. Adaptive optics could also be useful to correct the wavefront of the beam when propagating through turbid water with thermal inhomogeneity. Small beams, if not subject to bubbles, can outperform large-area beams in the case of vertical thermal gradient. Using a large receiving aperture can improve the system performance in the case of salinity. Our future research directions will include the use of reciprocity of turbulent channels to establish bi-directional high-performance underwater communications within real-sea conditions.

References

- [1] P. Lacovara, "High-bandwidth underwater communications," *Mar. Technol. Soc. J.*, vol. 42, no. 1, pp. 93–102, 2008.
- [2] H. Kaushal and G. Kaddoum, "Underwater optical wireless communication," *IEEE Access*, vol. 4, pp. 1518–1547, 2016.
- [3] J. Xu *et al.*, "Underwater wireless transmission of high-speed QAM-OFDM signals using a compact red-light laser," *Opt. Exp.*, vol. 24, pp. 8097–8109, 2016.
- [4] C. Shen *et al.*, "20-meter underwater wireless optical communication link with 1.5 Gbps data rate," *Opt. Exp.*, vol. 24, pp. 25502–25509, 2016.
- [5] X. Liu *et al.*, "34.5 m underwater optical wireless communication with 2.70 Gbps data rate based on a green laser diode with NRZ-OOK modulation," *Opt. Exp.*, vol. 25, pp. 27937–27947, 2017.
- [6] C. Fei, J. Zhang, G. Zhang, Y. Wu, X. Hong, and S. He, "Demonstration of 15-M 7.33-Gb/s 450-nm underwater wireless optical discrete multitone transmission using post nonlinear equalization," *J. Lightw. Technol.*, vol. 36, no. 3, pp. 728–734, Feb. 2018.
- [7] Y. Chen *et al.*, "26 m/5.5 Gbps air–water optical wireless communication based on an OFDM-modulated 520-nm laser diode," *Opt. Exp.*, vol. 25, pp. 14760–14765, 2017.
- [8] A. Wang *et al.*, "Adaptive water–air–water data information transfer using orbital angular momentum," *Opt. Exp.*, vol. 26, pp. 8669–8678, 2018.
- [9] J. Baghdady *et al.*, "Multi-gigabit/s underwater optical communication link using orbital angular momentum multiplexing," *Opt. Exp.*, vol. 24, pp. 9794–9805, 2016.
- [10] Y. Ren *et al.*, "Orbital angular momentum-based space division multiplexing for high-capacity underwater optical communications," *Sci. Rep.*, vol. 6, 2016, Art. no. 33306.
- [11] Y. Zhao *et al.*, "Demonstration of data-carrying orbital angular momentum-based underwater wireless optical multicasting link," *Opt. Exp.*, vol. 25, pp. 28743–28751, 2017.
- [12] L. C. Andrews and R. L. Phillips, *Laser Beam Propagation Through Random Media*, vol. 52. Bellingham, WA, USA: SPIE, 2005.
- [13] F. Hanson and M. Lasher, "Effects of underwater turbulence on laser beam propagation and coupling into single-mode optical fiber," *Appl. Opt.*, vol. 49, pp. 3224–3230, 2010.
- [14] H. M. Oubei *et al.*, "Simple statistical channel model for weak temperature-induced turbulence in underwater wireless optical communication systems," *Opt. Lett.*, vol. 42, pp. 2455–2458, 2017.
- [15] H. M. Oubei *et al.*, "Efficient Weibull channel model for salinity induced turbulent underwater wireless optical communications," in *Proc. Opto-Electron. Commun. Conf.*, Singapore, 2017, pp. 1–2.
- [16] H. M. Oubei, R. T. ElAfandy, K. H. Park, T. K. Ng, M.-S. Alouini, and B. S. Ooi, "Performance evaluation of underwater wireless optical communications links in the presence of different air bubble populations," *IEEE Photon. J.*, vol. 9, no. 2, Apr. 2017, Art. no. 7903009.
- [17] E. Zedini, H. M. Oubei, A. Kammoun, M. Hamdi, B. S. Ooi, and M.-S. Alouini, "A new simple model for underwater wireless optical channels in the presence of air bubbles," in *Proc. IEEE Global Commun. Conf.*, Singapore, 2017, pp. 1–6.
- [18] J. H. Shapiro, "Reciprocity of the turbulent atmosphere," *J. Opt. Soc. Amer.*, vol. 61, pp. 492–495, 1971.
- [19] D. L. Fried and H. T. Yura, "Telescope-performance reciprocity for propagation in a turbulent medium," *J. Opt. Soc. Amer.*, vol. 62, pp. 600–602, 1972.
- [20] R. R. Parenti, J. M. Roth, J. H. Shapiro, F. G. Walther, and J. A. Greco, "Experimental observations of channel reciprocity in single-mode free-space optical links," *Opt. Exp.*, vol. 20, pp. 21635–21644, 2012.
- [21] J. H. Shapiro and A. L. Puryear, "Reciprocity-enhanced optical communication through atmospheric turbulence—Part I: Reciprocity proofs and far-field power transfer optimization," *J. Opt. Commun. Netw.*, vol. 4, no. 12, pp. 947–954, Dec. 2012.
- [22] A. L. Puryear, J. H. Shapiro, and R. R. Parenti, "Reciprocity-enhanced optical communication through atmospheric turbulence—Part II: Communication architectures and performance," *J. Opt. Commun. Netw.*, vol. 5, no. 8, pp. 888–900, Aug. 2013.
- [23] C. J. Funk, "Multiple scattering calculations of light propagation in ocean water," *Appl. Opt.*, vol. 12, pp. 301–313, 1973.
- [24] W. Lu, L. Liu, and J. Sun, "Influence of temperature and salinity fluctuations on propagation behaviour of partially coherent beams in oceanic turbulence," *J. Opt. A, Pure Appl. Opt.*, vol. 8, pp. 1052–1058, 2006.
- [25] D. K. Woolf, J. H. Steele, S. A. Thorpe, and K. K. Turekian, "Bubbles," in *Encyclopedia of Ocean Sciences*. New York, NY, USA: Academic, 2001, pp. 352–357.
- [26] K. A. Mudge, K. K. M. B. D. Silva, B. A. Clare, K. J. Grant, and B. D. Nener, "Scintillation index of the free space optical channel: Phase screen modelling and experimental results," in *Proc. Int. Conf. Space Opt. Syst. Appl.*, Santa Monica, CA, USA, 2011, pp. 403–409.
- [27] J. Devore, *Probability and Statistics for Engineering and the Sciences*, 8th ed. Boston, MA, USA: Cengage Learning, 2011.
- [28] R. J. Hill, "Optical propagation in turbulent water," *J. Opt. Soc. Amer.*, vol. 68, no. 8, pp. 1067–1072, 1978.